ACS APPLIED MATERIALS & INTERFACES

Research Article

www.acsami.org

Carbon-, Binder-, and Precious Metal-Free Cathodes for Non-Aqueous Lithium−Oxygen Batteries: Nanoflake-Decorated Nanoneedle Oxide Arrays

Ahmer Riaz,[†,§] Kyu-Nam Jung,[‡] Wonyoung Chang,[∥] Kyung-Hee Shin,[‡] and Jong-Won Lee*[,†,§]

[†]New and Renewable Energy Research Division and [‡]Energy Efficiency and Materials Research Division, Korea Institute of Energy Research, 152 Gajeong-ro, Yuseong-gu, Daejeon 305-343, Republic of Korea

[§]Department of Advanced Energy Technology, Korea University of Science and Technology, 217 Gajeong-ro, Yuseong-gu, Daejeon 305-350, Republic of Korea

[∥]Center for Energy Convergence, Korea Institute of Science and Technology, Hwarangno, 14-gil 5, Seongbuk-gu, Seoul 136-791, Republic of Korea

Supporting Information

ABSTRACT: Rechargeable lithium−oxygen ($Li-O_2$) batteries have higher theoretical energy densities than today's lithium-ion batteries and are consequently considered to be an attractive energy storage technology to enable long-range electric vehicles. The main constituents comprising a cathode of a lithium−oxygen ($Li-O_2$) battery, such as carbon and binders, suffer from irreversible decomposition, leading to significant performance degradation. Here, carbon- and binder-free cathodes based on nonprecious metal oxides are designed and fabricated for $Li-O_2$ batteries. A novel structure of the oxide-only cathode having a high porosity and a large surface area is proposed that consists of numerous one-dimensional nanoneedle arrays decorated with thin nanoflakes. These oxide-only cathodes with the tailored architecture show high specific capacities and remarkably reduced charge potentials (in comparison with a carbon-only cathode) as well as excellent cyclability (250 cycles).

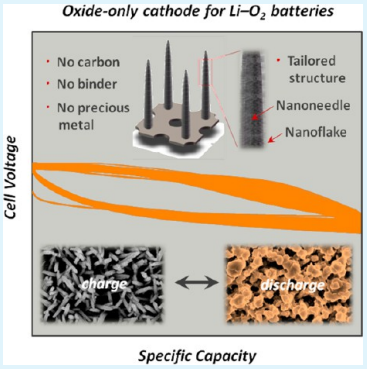

KEYWORDS: *lithium−oxygen battery, carbon, metal oxide array, nanoarchitecture, cyclability*

1. INTRODUCTION

The major hurdle for widespread commercialization of electric vehicles (EVs) is the low specific energies of present rechargeable batteries, which limit the vehicle's driving range. To propel EVs at driving ranges similar to gasoline-powered vehicles (e.g., >500 km), battery systems must have an energy density of more than 500 Wh kg^{-1}, which cannot be realized with current lithium-ion battery (LIB) technologies.[1,2] The growing demand for long-range EVs has led to considerable research and development activity of lithium−oxygen ($Li-O_2$) batteries that are expected to have several times higher energy densities than LIBs.[1−5]

A $Li-O_2$ battery delivers and stores electrical energy via the formation and decomposition of solid Li_2O_2 in a cathode (O_2 electrode), respectively. Significant progress has been made to improve the cathode's capacity, round-trip efficiency (i.e., reduce a discharge−charge voltage gap), and cycle life.[3−5] In most works reported so far, the cathode has been made of carbon and polymeric binders (typically, poly(vinylidene fluoride) (PVdF)) with catalysts in some cases. However, these main constituents have been known to be unstable in the presence of the discharge product (Li_2O_2) for the following reasons: (i) carbon reacts with Li_2O_2 to form Li_2CO_3 and other carbonate-like species that are difficult to oxidize on charging[6−8] and (ii) the PVdF binder undergoes the dehydrofluorination reaction that produces LiF and LiOH passivating the cathode surface.[9,10] Consequently, the accumulation of such byproducts leads to an increased charge voltage (i.e., reduced round-trip efficiency) as well as capacity decay over the course of discharge−charge cycling.

In recent years, a "carbon-free" cathode design has been proposed as a promising strategy to mitigate the carbon-induced problems. Au,[11] TiC,[12] or RuO_2 supported on indium tin oxide[13] was coated or pressed onto a current collector using polymeric binders and applied as a cathode. As a further step toward "binder-free" noncarbon cathodes, we also reported a Co_3O_4-only cathode directly grown on a current collector by the electrodeposition−conversion technique.[14] The carbon-free cathodes mentioned above have shown improved charging and cycling performance owing to reduced parasitic reactions, as compared with carbon-based cathodes.[11−14]

In addition to making cathodes chemically and electrochemically stable, tailoring cathode structures in nanoscale is of vital importance for high-performance $Li-O_2$ batteries. To develop

Received: July 8, 2014
Accepted: September 22, 2014
Published: October 3, 2014

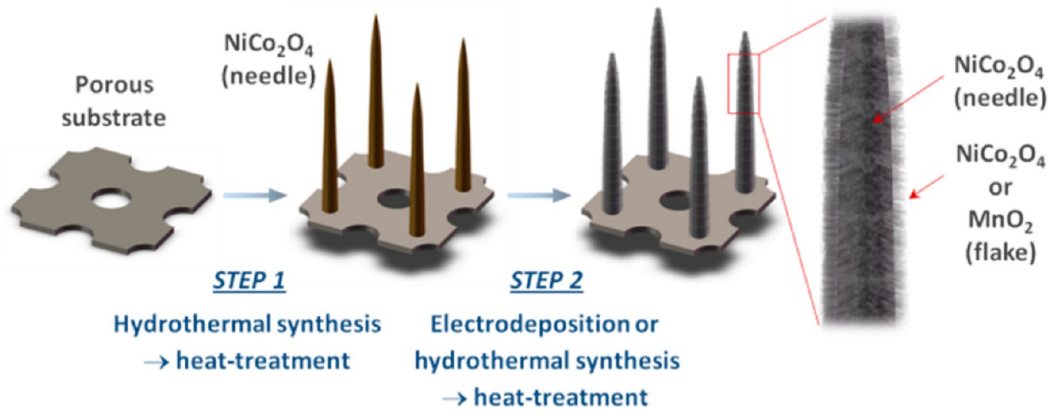

Figure 1. Two-step fabrication process of the oxide-only cathode consisting of the 1-D nanoneedle arrays decorated with nanoflakes. The cathode was directly deposited on a current collector without using carbon or binders.

a reversible Li−O_2 battery with a high specific capacity, a cathode structure should be designed and fabricated to have (i) a large number of active sites for O_2 reduction, (ii) a considerable amount of open space for Li_2O_2 storage, and (iii) an optimum porous structure that can facilitate mass transport. In fact, many of the earlier reports[15−20] on carbon-based cathodes have proven that properly tailored structures lead to improved storage capability and cyclability. Nanostructural engineering may be more critical for noncarbon cathodes that are usually made of much heavier and less porous materials (compared to carbon), but little effort has been invested to address this issue.

Herein, we report on an advanced cathode design based on transition metal oxides for Li−O_2 batteries with the following features: (i) the cathode does not contain carbon or polymeric binders; (ii) it does not have any precious metals such as Au and Ru; and (iii) it has a unique nanoarchitecture composed of numerous one-dimensional nanoneedle arrays decorated with thin nanoflakes. As will be shown later, the cathode presented here exhibits improved electrochemical performance (gravimetric capacity, round-trip efficiency, and cyclability) due to the absence of carbon and binders as well as the tailored nanostructure.

2. EXPERIMENTAL SECTION

2.1. Materials Synthesis. For preparation of $NiCo_2O_4$ nanoneedle arrays (step 1), a precursor solution was prepared by dissolving 0.4 mM $Co(NO_3)_2{\cdot}6H_2O$, 0.2 mM $Ni(NO_3)_2{\cdot}6H_2O$, and 0.75 mM urea ($(CO(NH_2)_2)$) in water. The resulting solution was transferred to a Teflon-lined stainless steel autoclave, and a piece of Ni foam was placed vertically in the solution. The autoclave was kept at 120 °C for 9 h. After that, the Ni foam was thoroughly washed with ethanol and water, then dried under vacuum at 80 °C, and, finally, heat-treated at 350 °C for 3 h. A typical loading value of $NiCo_2O_4$ deposited on the Ni foam was 0.3 mg cm^{-2}. $NiCo_2O_4$ nanoneedles were decorated with $NiCo_2O_4$ nanoflakes via electrodeposition (step 2) in a three-electrode cell in which the $NiCo_2O_4$-deposited Ni foam, a Pt mesh, and a Ag/AgCl electrode were used as the working, counter, and reference electrodes, respectively. The electrolyte used for the electrodeposition of $NiCo_2O_4$ nanoflakes was a mixed metal nitrate solution (33 mM $Ni(NO_3)_2{\cdot}6H_2O$ and 66 mM $Co(NO_3)_2{\cdot}6H_2O$). During the electrodeposition process, metal hydroxide is formed via electrochemical reduction of NO_3^- to OH^-, followed by precipitation:

$$NO_3^- + H_2O + 2e^- \rightarrow NO_2^- + 2OH^-, \quad E^\circ = -0.18\ \text{V vs Ag/AgCl} \tag{1}$$

$$M^{2+} + 2OH^- \rightarrow M(OH)_2 \quad (M = \text{Ni or Co}) \tag{2}$$

In this work, a constant potential of −0.5 V vs Ag/AgCl was applied for 5 min at room temperature to provide a sufficient overpotential for driving the electrochemical reduction reaction of nitrates while avoiding severe electrolysis of water. After electrodeposition, the specimen was rinsed with ethanol and water, followed by heat-treatment in air at 300 °C for 2 h. $NiCo_2O_4$ nanoneedles were decorated with MnO_2 nanoflakes by a hydrothermal method in a 2 mM $KMnO_4$ solution (step 2). The hydrothermal treatment was conducted at 150 °C for 1 h, and then, the specimen was washed with ethanol and water, and heat-treated in air at 350 °C for 3 h. The total mass of the $NiCo_2O_4$−$NiCo_2O_4$ and $NiCo_2O_4$−MnO_2 electrodes was 0.6 mg cm^{-2}. For preparation of carbon nanotube (CNT) buckypapers, the CNTs (50 mg) were dispersed in deionized water (50 mL) with Triton X-100 (500 mg) as a surfactant and then sonicated for 1 h. The well-dispersed CNT suspension was filtered through a polytetrafluoroethylene (PTFE) membrane with a 0.22 μm pore diameter under vacuum and washed with water and methanol to remove any remaining surfactant. The resulting CNT buckypaper was peeled off of the PTFE membrane and dried under vacuum at 60 °C for 12 h. The weight of the CNT buckypaper was ca. 0.6 mg cm^{-2}.

2.2. Electrochemical Experiments. The Li−O_2 battery was composed of a Li metal anode, an electrolyte (1 M lithium bis(trifluoromethane-sulfonyl)imide (LiTFSI) in tetraethylene glycol dimethyl ether (TEGDME)) impregnated into a glass fiber separator, and a cathode with an active area of 0.785 cm^2. Discharge−charge profiles were measured at a current density of 50 mA g^{-1}. The cycling test was performed with a 500 mAh g^{-1} capacity at 100 mA g^{-1} using a Maccor Series 4000. The ac-impedance spectra were measured from 10^6 to 0.01 Hz with an ac signal of 5 mV amplitude using a Zhaner Zennium. The potentiostatic intermittent titration technique (PITT) was used to study the charging behavior. Batteries were discharged galvanostatically to 1000 mAh g^{-1} at a rate of 20 mA g^{-1}, then rested for 1 h, and finally charged using a PITT protocol with a 12 mV potential step. The cutoff current value used for the PITT experiments was either 12.5 mA g^{-1} or 32.0 mA g^{-1}, depending on the cathode. In this report, all of the gravimetric capacities and current densities were calculated based on the total oxide mass.

2.3. Materials Characterization. To identify the crystal structures, X-ray diffraction (XRD) patterns were recorded with an automated Rigaku diffractometer (2500 D/MAX, Rigaku) using Cu Kα (λ = 1.5405 Å) radiation. The measurements were conducted over the scanning angle range of 10−90° at a scan rate of 5° min^{-1}. The morphology and microstructure were examined by scanning electron microscopy (SEM, Hitach X-4900) and transmission electron microscopy (TEM, Hitachi H9000). The Brunauer−Emmett−Teller (BET) surface area was determined from N_2 sorption isotherms by using a BEL-SORP mini system. X-ray photoelectron spectroscopy

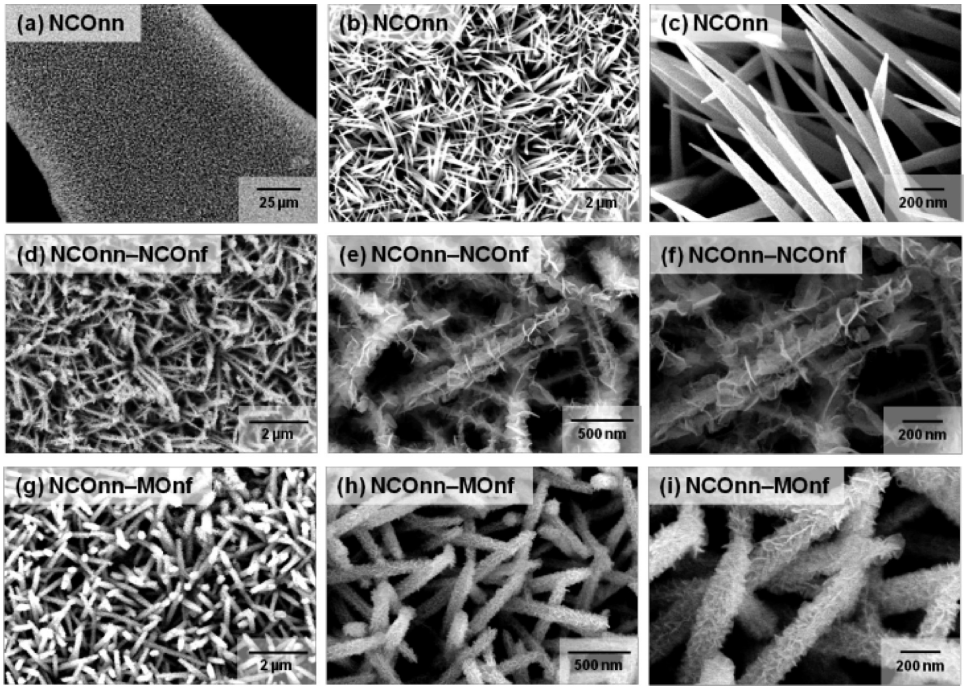

Figure 2. SEM micrographs of the oxide-only cathodes: (a–c) $NiCo_2O_4$ nanoneedle (NCOnn); (d–f) $NiCo_2O_4$ nanoneedle (NCOnn) decorated with $NiCo_2O_4$ nanoflake (NCOnf); (g–i) $NiCo_2O_4$ nanoneedle (NCOnn) decorated with MnO_2 nanoflake (MOnf).

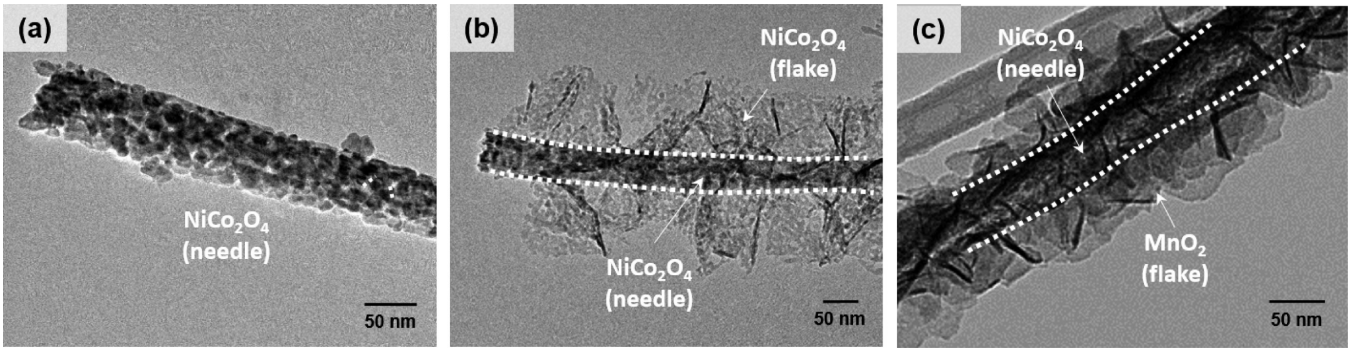

Figure 3. TEM micrographs of (a) NCOnn, (b) NCOnn–NCOnf, and (b) NCOnn–MOnf.

(XPS) was conducted using a Thermo MultiLab 2000 spectrometer with a monochromatic Al Kα X-ray source.

3. RESULTS AND DISCUSSION

Unlike conventional methods for cathode preparation, in the present study, oxide cathodes were directly deposited onto a porous current collector without using any carbon or binders. Among various types of oxides proposed for Li–O_2 batteries, transition metal oxides based on Co, Ni, and Mn were used in this work because of their high catalytic activity and low cost.[21−24] A schematic overview of the fabrication procedure of the cathode is illustrated in Figure 1. First, $NiCo_2O_4$ nanoneedles were prepared on a conducting substrate (Ni foam) via a hydrothermal reaction in a mixed solution of metal nitrates and urea, followed by heat-treatment (step 1). The hydrolysis of urea releases ammonia and carbonic acid that reacts with metal ions to form nanoneedle-like metal carbonate (see the SEM images in SI Figure S1).[25] When thermally annealed in air, the metal carbonate is converted to $NiCo_2O_4$. The hydrothermal conditions were carefully controlled to obtain 1-D nanoneedle arrays with desired density and thickness.

Next, the $NiCo_2O_4$ nanoneedles were decorated with nanoflakes by either electrochemical or hydrothermal synthesis (step 2). The $NiCo_2O_4$ nanoflakes were electrochemically deposited onto the $NiCo_2O_4$ nanoneedles in a metal nitrate solution, followed by heat-treatment. The electrodeposition process leads to the precipitation of metal hydroxide.[26−28] The hydroxide is then converted to $NiCo_2O_4$ by thermal annealing in air. Alternatively, MnO_2 nanoflakes were coated onto the $NiCo_2O_4$ nanoneedles by a well-known hydrothermal process from a $KMnO_4$ solution[29] and subsequent heat-treatment. The XRD (SI Figure S2) and XPS (SI Figure S3) analyses confirmed that spinel $NiCo_2O_4$ nanoneedles with spinel $NiCo_2O_4$ or birnessite MnO_2 nanoflakes were successfully synthesized by the two-step fabrication process. The total mass of the nanoflake-decorated nanoneedle cathode is 0.6 mg cm^{-2}. For simplicity, $NiCo_2O_4$ nanoneedle, $NiCo_2O_4$ nanoflake, and MnO_2 nanoflake will hereafter be referred to as NCOnn, NCOnf, and MOnf, respectively.

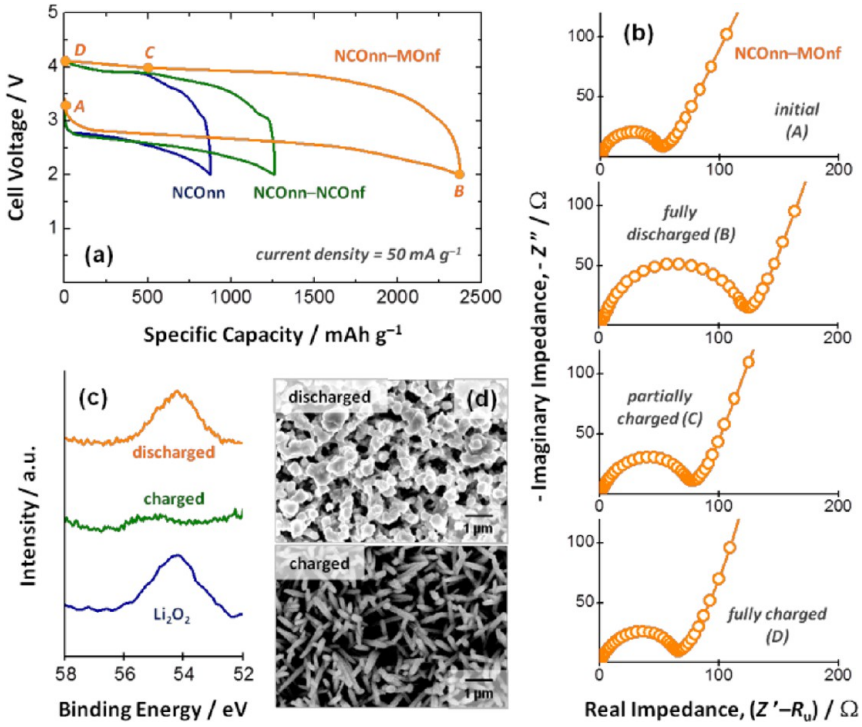

Figure 4. (a) Discharge–charge profiles of the oxide-only cathodes. The electrolyte was 1 M LiTFSI in TEGDME. (b) ac-impedance spectra of the NCOnn–MOnf cathode at the points denoted as A–D in part a. The measured real impedance (Z') was subtracted by the uncompensated ohmic resistance R_U. (c) Li 1s XPS spectra and (d) SEM micrographs for the discharged and charged NCOnn–MOnf cathodes. The reference XPS spectrum for Li_2O_2 is also shown in part c.

Figure 2(a–c) shows SEM images of the NCOnn arrays synthesized by step 1. Numerous 1-D nanoneedles (<100 nm in diameter) have completely covered the entire surface of the substrate and formed a highly porous architecture. Note that the conical nanoneedles have very smooth surfaces (Figure 2c). The SEM micrographs of the NCOnn arrays decorated with NCOnf and MOnf in step 2 are presented in Figure 2(d–f and g–i), respectively. It is clearly seen that NCOnf and MOnf were conformally coated along the NCOnn surface, leading to a significant increase in surface roughness. No large-scale agglomerates of $NiCo_2O_4$ or MnO_2 were formed so that the original, highly porous structures were preserved even after the nanoflake decoration. The structures of the nanoflake-decorated nanoneedle arrays were further examined by TEM. The TEM images in Figure 3 confirm the core–shell-like structures of NCOnn–NCOnf and NCOnn–MOnf. Both the NCOnf and MOnf deposited on NCOnn appear very thin, as indicated by their transparent characteristics in the TEM micrographs. There may be a concern about use of the Ni foam as a substrate (current collector) for Li–O_2 batteries, because of possible parasitic reactions on the Ni surface. As shown in Figure 2a, the entire surface of the Ni foam was completely covered with the oxide nanoneedles; that is, the surface coverage of Ni would be quite small. Furthermore, bare Ni, if any, might have been transformed to nickel oxides upon heat-treatment, and nickel oxides are known to improve the interfacial stability between the Ni foam and the electrolyte.[30]

We expect that the cathode design proposed here can make notable improvements to the performance of Li–O_2 batteries due to the following features: (i) the cathodes do not contain carbon or binders that decompose and thus reduce the battery reversibility; (ii) they have a large amount of pores among the 1-D nanoneedles that can be utilized for Li_2O_2 storage; and (iii) they have high surface areas due to the presence of nanoflakes on nanoneedles, that is, a large number of active reaction sites (Li_2O_2 nucleation sites). Moreover, no precious metals were incorporated into the cathode, providing an additional benefit in cost.

Li–O_2 batteries were built and tested using the oxide-only cathodes with the nanoflake-decorated nanoneedle arrays. Figure 4a presents typical discharge–charge curves of the Li–O_2 batteries assembled with the three different cathodes (NCOnn, NCOnn–NCOnf, and NCOnn–MOnf). Here, the data were measured at a current density of 50 mA g^{-1} based on the total oxide mass. One M LiTFSI in TEGDME was used as an electrolyte since TEGDME is less prone to attack by reduced oxygen radicals as compared with carbonate-based solvents.[31,32] All of the cathodes exhibit discharge potentials as high as 2.6–2.8 V vs Li/Li^+, followed by a gradual decrease down to 2.0 V vs Li/Li^+ with increasing depth of discharge. Then, the cathodes can be fully charged at potentials lower than 4.0 V vs Li/Li^+. Both of the NCOnn–NCOnf and NCOnn–MOnf cathodes exhibit similar discharge–charge potentials, which suggests that there is no considerable difference between the catalytic properties of $NiCo_2O_4$ and MnO_2.

Furthermore, the ac-impedance spectra of the NCOnn–MOnf cathode measured during discharge and charge (designated as A–D in Figure 4a) are shown in Figure 4b. The measured real impedance (Z') was subtracted by the uncompensated ohmic resistance R_U. Each of the impedance spectra consists of a slightly depressed arc in the high-frequency range and a straight line inclined at a constant angle to the real axis in the low-frequency range. The high-frequency arc is attributed to the interfacial polarization reaction, and a straight line at low frequencies is associated with oxygen diffusion (i.e., Warburg impedance).[33] The interfacial polarization resistance

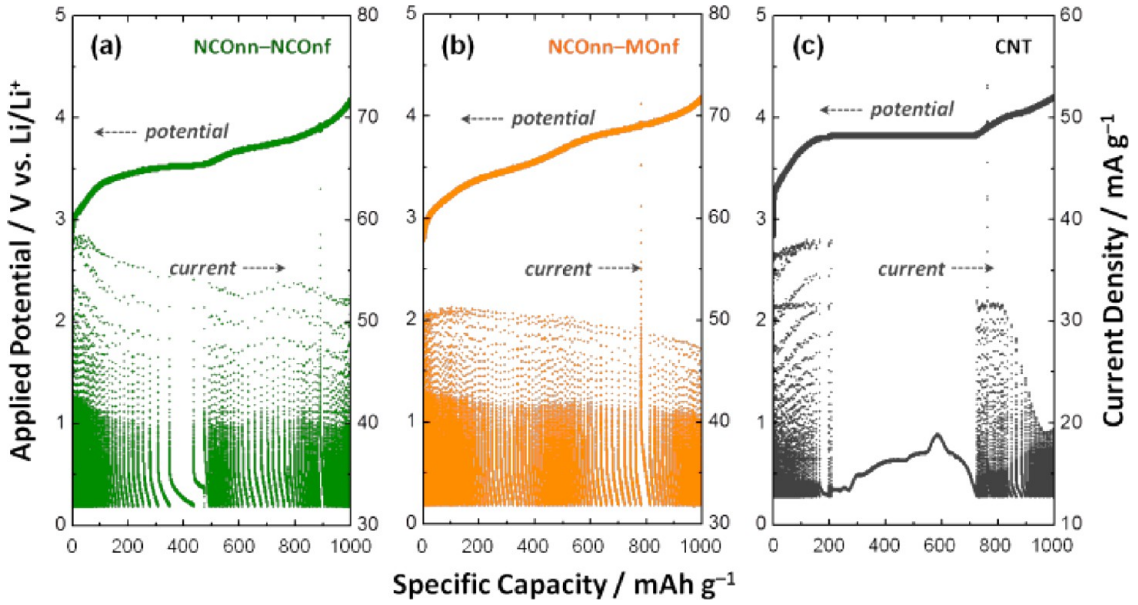

Figure 5. Charge profiles of the (a) NCOnn–NCOnf, (b) NCOnn–MOnf cathodes, and (c) the carbon (CNT)-only cathode obtained by PITT. The cathodes were galvanostatically discharged to a 1000 mAh g^{-1} capacity prior to the PITT charging.

increased from 53 Ω to 126 Ω upon discharging, which indicates the formation of resistive discharge products on the cathode surface. After charging, the polarization resistance decreased to a level similar to the initial value, suggesting the reversibility of discharge–charge reactions.

The discharged and charged cathodes were analyzed by XPS and SEM to identify the discharge products as well as to examine the reversibility of the electrochemical reactions. Figure 4c shows XPS spectra of the Li 1s region for the discharged and charged NCOnn–MOnf cathodes. In the XPS data of the discharged cathode, a peak is observed at a binding energy of 54.2 eV, which is consistent with the previous reports on electrochemically produced Li_2O_2 species.[13,34,35] This confirms that the major discharge product is Li_2O_2. The characteristic peak for Li_2O_2 disappeared from the XPS data of the charged cathode, indicating that Li_2O_2 decomposed upon subsequent charging. The reversible formation and decomposition of Li_2O_2 was further supported by the SEM observations. As shown in Figure 4d, the discharge products were uniformly deposited on the surface of the NCOnn–MOnf arrays, resulting in a reduced porosity, and they were then removed during the charging process. The experimental results confirm that the oxide-only cathodes free of carbon and binders can be discharged and charged via the formation and decomposition of Li_2O_2 (considered to be the desired reaction pathway), respectively.

At this point, we make the following remarks concerning the electrochemical behaviors of the oxide-only cathodes (Figure 4a). First, the decoration of nanoneedles with nanoflakes leads to a considerable improvement in the discharge capacity. The specific capacity (calculated based on the total oxide mass and the geometric electrode area) increases in the order of NCOnn (876 mAh g^{-1} and 263 μAh cm^{-2}) < NCOnn–NCOnf (1261 mAh g^{-1} and 757 μAh cm^{-2}) < NCOnn–MOnf (2372 mAh g^{-1} and 1423 μAh cm^{-2}), which follows the trend in surface area. The surface areas were measured to be 111 m^2 g^{-1} for NCOnn, 180 m^2 g^{-1} for NCOnn–NCOnf, and 387 m^2 g^{-1} for NCOnn–MOnf by BET analysis (SI Figure S4). When normalized by their BET surface areas, the three different cathodes delivered similar specific capacities in the range of 0.61–0.79 μAh cm^{-2}, indicating a strong correlation between the surface area and the capacity.

In principle, the capacity of a Li–O_2 battery cathode should be exclusively determined by the pore volume available for Li_2O_2 accumulation rather than by the surface area. However, the formation of resistive Li_2O_2 species during discharge could severely increase the internal resistance and hence cause a premature death even before the available pores are completely filled with Li_2O_2. Such a hypothesis is fully supported by the galvanostatic discharge and ac-impedance data as well as the SEM characterization in Figure 4. In this case, the surface area plays the dominant role in determining a capacity at a given discharge rate. Here, we demonstrate that the decoration of nanoneedles with nanoflakes remarkably improves the specific capacity by increasing the number of active sites for O_2 reduction on the cathode, while preserving the highly porous structure of the nanoneedle arrays. As shown in this paper, the surface area is one of the most important factors that determine the discharge capacity. Furthermore, our previous study[14] demonstrated that the nanoneedle-like Co_3O_4 cathode with vertical porous channels exhibited better cycling performance in comparison to the nanosheet- and nanoflower-like cathodes with tortuous pores. This suggests that vertical channels provide open frameworks that can faciliatate effective mass transport and uniform Li_2O_2 deposition, thereby improving electrochemical performance.

Second, the charge potentials of the oxide-only cathodes appear to be lower in comparison with those values commonly reported on carbon-based cathodes. We performed more detailed characterization of the charging behavior using a potentiostatic intermittent titration technique (PITT), as suggested by Lu and Shao-Horn.[36] The PITT experiment employs a small potential step to drive an electrochemical reaction, and hence, it provides more useful information on charging behaviors under quasi-equilibrium conditions. The Li–O_2 batteries were galvanostatically discharged to 1000 mAh g^{-1} at a rate of 20 mA g^{-1}, and then they were charged using a PITT protocol with a 12 mV step. Figure 5(a and b) displays

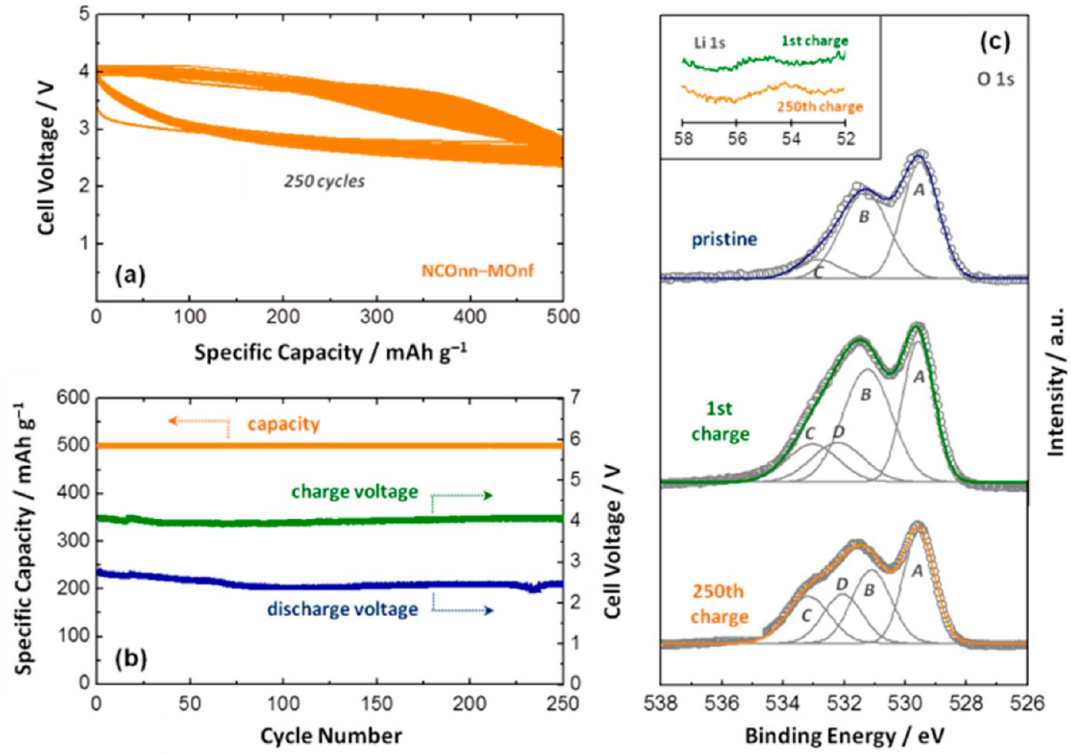

Figure 6. (a) Discharge–charge profiles of the NCOnn–MOnf cathode measured for 250 cycles at 100 mA g^{-1} and (b) the plots of capacity and discharge and charge voltages vs cycle number. (c) O 1s XPS spectra for the pristine and tested NCOnn–MOnf cathodes (after first and 250th charge). The inset in part c shows the Li 1s XPS spectra.

the PITT charge profiles for the NCOnn–NCOnf and NCOnn–MOnf cathodes, respectively, along with the measured anodic currents at each of the applied potential steps. For comparison, data for a carbon-only cathode were also measured and are presented in Figure 5c. Here, the carbon-only cathode was prepared as a thin sheet of CNTs (buckypaper) without using any binders. The buckypaper-type carbon cathode was chosen because it allowed us to minimize complications related to binders and to make an equivalent comparative evaluation of the charging behaviors of oxides and carbon.

The PITT charge curves for the NCOnn–NCOnf and NCOnn–MOnf cathodes exhibited a continuous potential increase during charge. It should be pointed out that the NCOnn–NCOnf and NCOnn–MOnf cathodes deliver ca. 82% and 61% of the total charge capacity, respectively, at potentials lower than 3.8 V vs Li/Li$^+$. On the other hand, the carbon-only cathode displays a large potential plateau at 3.8 V vs Li/Li$^+$ below which only 17% of the total charge capacity is delivered. Such high charge potentials of the carbon-only cathode may be largely due to the presence of Li_2CO_3 species formed as a result of the parasitic reaction between carbon and Li_2O_2 as mentioned before. McCloskey et al.[6] suggested that thin carbonate layers at the carbon/Li_2O_2 interface cause a significant reduction in the exchange current density, leading to a large potential increase during charge. Our PITT experiments prove that the oxide-only cathodes show remarkably lower charge potentials as compared with the carbon-only cathode. Moreover, the anodic current values measured on NCOnn–NCOnf and NCOnn–MOnf were observed to be comparable to or even higher than those for carbon, indicating facile reaction kinetics on the oxide cathodes. These observations suggest that the oxide-only cathodes based on nanoflake-decorated nanoneedle arrays are more stable in the presence of Li_2O_2, leading to reduced formation of carbonates and thus decreased charge potentials.

The NCOnn–MOnf cathode with the highest capacity was employed for a long-term cyclability test. The cycling performance of the NCOnn–MOnf cathode at a current density of 100 mA g^{-1} is presented in Figure 6a. The NCOnn–MOnf cathode could be discharged and charged with a limited capacity of 500 mAh g^{-1} for at least 250 cycles. No significant changes in the discharge–charge profiles were observed over the course of repeated cycles. Figure 6b illustrates the capacity and the terminal discharge and charge voltages as a function of the cycle number. In addition to the capacity retention for 250 cycles, the battery showed no remarkable increase in the discharge–charge voltage gap.

To examine possible changes in the cathode composition during cycling, we disassembled the battery after the cycling test and then analyzed the cycled cathode using XPS. Figure 6c compares the XPS spectra of the O 1s region for the pristine and cycled cathodes. The observed spectrum of the pristine cathode was deconvoluted into three component curves (A, B, and C). The low binding energy peak at 529.6 eV (A) is ascribed to the metal–oxygen bond in the metal oxides. The peak at 531.2 eV (B) is generally associated with defects, contaminants, and a number of surface species including hydroxyls, chemisorbed oxygen, and under-coordinated lattice oxygen. The high binding energy peak at 533.1 eV (C) originates from the multiplicity of physi- and/or chemi-sorbed water molecules at the surface.[37−39] The XPS spectra of the cathodes at the end of first and 250th charges show an additional peak at 532.1 eV (D) that can be attributed to carbonate species. We speculate that a small amount of carbonate species may have resulted from parasitic electrolyte (TEGDME) decomposition.[6−8] It should be noted, however,

that the peak area ratios (D/A) for the charged cathodes were determined to be similar: 0.46 for first charge and 0.54 for 250th charge. Also, no large signals for carbonate species were detected from the Li 1s XPS spectra (see the inset in Figure 6c). These results suggest that the accumulation of carbonates on the oxide-only cathode is insignificant even after 250 cycles and that the cathode remains stable.

4. CONCLUSION

Carbon- and binder-free cathodes based on nonprecious metal oxides were directly fabricated on a porous conducting substrate and applied as cathodes for rechargeable Li−O_2 batteries. The cathode architecture incorporates a unique design feature that consists of one-dimensional nanoneedle arrays decorated with thin nanoflakes. The oxide-only cathodes deliver a high specific capacity, as high as 2372 mAh g^{-1}, and lower charge potentials compared to carbon as well as stable performance for 250 cycles. The excellent electrochemical performance can be explained by the fact that (i) the carbon- and binder-free cathode is stable against the parasitic reaction with Li_2O_2 and thus promotes reversible formation and decomposition of Li_2O_2; (ii) pores among 1-D nanoneedles offer a large amount of open spaces for Li_2O_2 accumulation, while reducing mass transport limitations; and (iii) the nanoflakes deposited on nanoneedles provide a large number of active reaction sites. In addition to the significance of the carbon- and binder-free cathode design, this report conveys an important message that nanostructural engineering of non-carbon cathodes is very crucial for developing high-performance Li−O_2 batteries.

■ ASSOCIATED CONTENT

Supporting Information

SEM, XRD, XPS, and BET analyses. This material is available free of charge via the Internet at http://pubs.acs.org.

■ AUTHOR INFORMATION

Corresponding Author

*Tel.: +82-42-860-3025. Fax.: +82-42-860-3297. Email: jjong277@kier.re.kr.

Notes

The authors declare no competing financial interest.

■ ACKNOWLEDGMENTS

This work was supported by a Research and Development Program of the Korea Institute of Energy Research (KIER B4-2481-05) grant and by an Energy Efficiency & Resources Core Technology Program of the Korea Institute of Energy Technology Evaluation and Planning (KETEP), granted financial resource from the Ministry of Trade, Industry & Energy, Republic of Korea. (No. 20112020100110/KIER B4-2462).

■ REFERENCES

(1) Christensen, J.; Albertus, P.; Sanchez-Carrera, R. S.; Lohmann, Y.; Kozinsky, B.; Liedtke, R.; Ahmed, J.; Kojic, A. A Critical Review of Li/Air Batteries. *J. Electrochem. Soc.* **2012**, *159*, R1−R30.

(2) Park, M. S.; Ma, S. B.; Lee, D. J.; Im, D.; Doo, S.-G.; Yamamoto, O. A Highly Reversible Lithium Metal Anode. *Sci. Rep.* **2014**, *4:3815*, 1−8.

(3) Girishkumar, G.; McCloskey, B.; Luntz, A. C.; Swanson, S.; Wilcke, W. Lithium−Air Battery: Promise and Challenges. *J. Phys. Chem. Lett.* **2010**, *1*, 2193−2203.

(4) Li, F.; Zhang, T.; Zhou, H. Challenges of Non-Aqueous Li−O_2 Batteries: Electrolytes, Catalysts, and Anodes. *Energy Environ. Sci.* **2013**, *6*, 1125−1141.

(5) Lu, J.; Li, L.; Park, J.-B.; Sun, Y.-K.; Wu, F.; Amine, K. Aprotic and Aqueous Li−O_2 Batteries. *Chem. Rev.* **2014**, *114*, 5611−5640.

(6) McCloskey, B. D.; Speidel, A.; Scheffler, R.; Miller, D. C.; Viswanathan, V.; Hummelshøj, J. S.; Nørskov, J. K.; Luntz, A. C. Twin Problems of Interfacial Carbonate Formation in Nonaqueous Li−O_2 Batteries. *J. Phys. Chem. Lett.* **2012**, *3*, 997−1001.

(7) Gallant, B. M.; Mitchell, R. R.; Kwabi, D. G.; Zhou, J.; Zuin, L.; Thompson, C. V.; Shao-Horn, Y. Chemical and Morphological Changes of Li−O_2 Battery Electrodes upon Cycling. *J. Phys. Chem. C* **2012**, *116*, 20800−20805.

(8) Ottakam Thotiyl, M. M.; Freunberger, S. A.; Peng, Z.; Bruce, P. G. The Carbon Electrode in Nonaqueous Li−O_2 Cells. *J. Am. Chem. Soc.* **2013**, *135*, 494−500.

(9) Black, R.; Oh, S. H.; Lee, J.-H.; Yim, T.; Adams, B.; Nazar, L. F. Screening for Superoxide Reactivity in Li−O_2 Batteries: Effect on Li_2O_2/LiOH Crystallization. *J. Am. Chem. Soc.* **2012**, *134*, 2902−2905.

(10) Nasybulin, E.; Xu, W.; Engelhard, M. H.; Nie, Z.; Li, X. S.; Zhang, J.-G. Stability of Polymer Binders in Li−O_2 Batteries. *J. Power Sources* **2013**, *243*, 899−907.

(11) Peng, Z.; Freunberger, S. A.; Chen, Y.; Bruce, P. G. A Reversible and Higher-Rate Li−O_2 Battery. *Science* **2012**, *337*, 563−566.

(12) Ottakam Thotiyl, M. M.; Freunberger, S. A.; Peng, Z.; Chen, Y.; Liu, Z.; Bruce, P. G. A Stable Cathode for the Aprotic Li−O_2 Battery. *Nat. Mater.* **2013**, *12*, 1050−1056.

(13) Li, F.; Tang, D.-M.; Chen, Y.; Golberg, D.; Kitaura, H.; Zhang, T.; Yamada, A.; Zhou, H. Ru/ITO: A Carbon-Free Cathode for Nonaqueous Li−O_2 Battery. *Nano Lett.* **2013**, *13*, 4702−4707.

(14) Riaz, A.; Jung, K.-N.; Chang, W.; Lee, S.-B.; Lim, T.-H.; Park, S.-J.; Song, R.-H.; Yoon, S.; Shin, K.-H.; Lee, J.-W. Carbon-Free Cobalt Oxide Cathodes with Tunable Nanoarchitectures for Rechargeable Lithium−Oxygen Batteries. *Chem. Commun.* **2013**, *49*, 5984−5986.

(15) Wang, Z.-L.; Xu, D.; Xu, J.-J.; Zhang, L.-L.; Zhang, X.-B. Graphene Oxide Gel-Derived, Free-Standing, Hierarchically Porous Carbon for High-Capacity and High-Rate Rechargeable Li−O_2 Batteries. *Adv. Funct. Mater.* **2012**, *22*, 3699−3705.

(16) Lim, H.-D.; Park, K.-Y.; Song, H.; Jang, E. Y.; Gwon, H.; Kim, J.; Kim, Y. H.; Lima, M. D.; Ovalle Robles, R.; Lepró, X.; Baughman, R. H.; Kang, K. Enhanced Power and Rechargeability of a Li−O_2 Battery Based on a Hierarchical-Fibril CNT Electrode. *Adv. Mater.* **2013**, *25*, 1348−1352.

(17) Guo, Z.; Zhou, D.; Dong, X. L.; Qiu, Z.; Wang, Y.; Xia, Y. Ordered Hierarchical Mesoporous/Macroporous Carbon: A High-Performance Catalyst for Rechargeable Li−O_2 Batteries. *Adv. Mater.* **2013**, *25*, 5668−5672.

(18) Lin, X.; Zhou, L.; Huang, T.; Yu, A. Hierarchically Porous Honeycomb-Like Carbon as a Lithium−Oxygen Electrode. *J. Mater. Chem. A* **2013**, *1*, 1239−1245.

(19) Chen, Y.; Li, F.; Tang, D.-M.; Jian, Z.; Liu, C.; Golberg, D.; Yamada, A.; Zhou, H. Multi-Walled Carbon Nanotube Papers as Binder-Free Cathodes for Large Capacity and Reversible Non-Aqueous Li−O_2 Batteries. *J. Mater. Chem. A* **2013**, *1*, 13076−13081.

(20) Shui, J.; Du, F.; Xue, C.; Li, Q.; Dai, L. Vertically Aligned N−Doped Coral-Like Carbon Fiber Arrays as Efficient Air Electrodes for High-Performance Nonaqueous Li−O_2 Batteries. *ACS Nano* **2014**, *8*, 3015−3022.

(21) Zhang, L.; Zhang, S.; Zhang, K.; Xu, G.; He, X.; Dong, S.; Liu, Z.; Huang, C.; Gu, L.; Cui, G. Mesoporous $NiCo_2O_4$ Nanoflakes as Electrocatalysts for Rechargeable Li−O_2 Batteries. *Chem. Commun.* **2013**, *49*, 3540−3542.

(22) Black, R.; Lee, J.-H.; Adams, B.; Mims, C. A.; Nazar, L. F. The Role of Catalysts and Peroxide Oxidation in Lithium−Oxygen Batteries. *Angew. Chem., Int. Ed.* **2013**, *125*, 410−414.

(23) Oh, D.; Qi, J.; Lu, Y.-C.; Zhang, Y.; Shao-Horn, Y.; Belcher, A. M. Biologically Enhanced Cathode Design for Improved Capacity and Cycle Life for Lithium−Oxygen Batteries. *Nat. Commun.* **2013**, *4:2756*, 1−8.

(24) Ryu, W.-H.; Yoon, T.-H.; Song, S. H.; Jeon, S.; Park, Y.-J.; Kim, I.-D. Bifunctional Composite Catalysts Using Co_3O_4 Nanofibers Immobilized on Nonoxidized Graphene Nanoflakes for High-Capacity and Long-Cycle Li−O_2 Batteries. *Nano Lett.* **2013**, *13*, 4190−4197.
(25) Bastakoti, B. P.; Kamachi, Y.; Huang, H.-S.; Chen, L.-C.; Wu, K. C.-W.; Yamauchi, Y. Hydrothermal Synthesis of Binary Ni−Co Hydroxides and Carbonate Hydroxides as Pseudosupercapacitors. *Eur. J. Inorg. Chem.* **2013**, *2013*, 39−43.
(26) Yang, G.-W.; Xu, C.-L.; Li, H.-L. Electrodeposited Nickel Hydroxide on Nickel Foam with Ultrahigh Capacitance. *Chem. Commun.* **2008**, 6537−6539.
(27) Xia, X. H.; Tu, J. P.; Zhang, Y. Q.; Mai, Y. J.; Wang, X. L.; Gu, C. D.; Zho, X. B. Three-Dimensional Porous Nano-Ni/$Co(OH)_2$ Nanoflake Composite Film: A Pseudocapacitive Material with Superior Performance. *J. Phys. Chem. C* **2011**, *115*, 22662−22668.
(28) Huang, L.; Chen, D.; Ding, Y.; Feng, S.; Wang, Z. L.; Liu, M. Nickel−Cobalt Hydroxide Nanosheets Coated on $NiCo_2O_4$ Nanowires Grown on Carbon Fiber Paper for High-Performance Pseudocapacitors. *Nano Lett.* **2013**, *13*, 3135−3139.
(29) Wei, W.; Cui, X.; Chen, W.; Ivey, D. G. Manganese Oxide-Based Materials as Electrochemical Supercapacitor Electrodes. *Chem. Soc. Rev.* **2011**, *40*, 1697−1721.
(30) Liu, X.; Wang, D.; Shi, S. Exploration on the Possibility of Ni Foam as Current Collector in Rechargeable Lithium−Air Batteries. *Electrochim. Acta* **2013**, *87*, 865−871.
(31) McCloskey, B. D.; Bethune, D. S.; Shelby, R. M.; Girishkumar, G.; Luntz, A. C. Solvents' Critical Role in Non-Aqueous Lithium−Oxygen Battery Electrochemistry. *J. Phys. Chem. Lett.* **2011**, *2*, 1161−1166.
(32) Jung, H.-G.; Hassoun, J.; Park, J.-B.; Sun, Y.-K.; Scrosati, B. An Improved High-Performance Lithium−Air Battery. *Nat. Chem.* **2012**, *4*, 579−585.
(33) Mirzaeian, M.; Hall, P. J. Characterizing Capacity Loss of Lithium Oxygen Batteries by Impedance Spectroscopy. *J. Power Sources* **2010**, *195*, 6817−6824.
(34) Lu, Y.-C.; Crumlin, E. J.; Veith, G. M.; Harding, J. R.; Mutoro, E.; Baggetto, L.; Dudney, N. J.; Liu, Z.; Shao-Horn, Y. In Situ Ambient Pressure X-ray Photoelectron Spectroscopy Studies of Lithium−Oxygen Redox Reactions. *Sci. Rep.* **2012**, *2:715*, 1−6.
(35) Li, J.; Zou, M.; Chen, L.; Huang, Z.; Guan, L. An Efficient Bifunctional Catalyst of Fe/Fe_3C Carbon Nanofibers for Rechargeable Li−O_2 Batteries. *J. Mater. Chem. A* **2014**, *2*, 10634−10638.
(36) Lu, Y.-C.; Shao-Horn, Y. Probing the Reaction Kinetics of the Charge Reactions of Nonaqueous Li−O_2 Batteries. *J. Phys. Chem. Lett.* **2013**, *4*, 93−99.
(37) Li, J.; Xiong, S.; Liu, Y.; Ju, Z.; Qian, Y. High Electrochemical Performance of Monodisperse $NiCo_2O_4$ Mesoporous Microspheres as an Anode Material for Li-Ion Batteries. *ACS Appl. Mater. Interfaces* **2013**, *5*, 981−988.
(38) Thissen, A.; Ensling, D.; Madrigal, F. J. F.; Jaegermann, W. Photoelectron Spectroscopic Study of the Reaction of Li and Na with $NiCo_2O_4$. *Chem. Mater.* **2005**, *17*, 5202−5208.
(39) Kim, J.-G.; Pugmire, D. L.; Battaglia, D.; Langell, M. A. Analysis of the $NiCo_2O_4$ Spinel Surface with Auger and X-ray Photoelectron Spectroscopy. *Appl. Surf. Sci.* **2000**, *165*, 70−84.